

Molecular dynamics of flows in the Knudsen regime

MAREK CIEPLAK¹, JOEL KOPLIK² & JAYANTH R. BANAVAR³

¹ *Institute of Physics, Polish Academy of Sciences, 02-668 Warsaw, Poland*

² *Benjamin Levich Institute and Department of Physics, City College of New York, NY 10031*

³ *Department of Physics and Center for Materials Physics, 104 Davey Laboratory, The Pennsylvania State University, University Park, Pennsylvania 16802*

Novel technological applications often involve fluid flows in the Knudsen regime in which the mean free path is comparable to the system size. We use molecular dynamics simulations to study the transition between the dilute gas and the dense fluid regimes as the fluid density is increased.

PACS numbers: 51.10.+y, 34.10.+x, 92.20.Bk

In a landmark paper [1], Maxwell applied his kinetic theory [2] to the study of the slip length associated with fluid flow close to a solid surface. He postulated a linear combination of two kinds of behaviour when a molecule was incident on a wall – it is either specularly reflected or it undergoes enough collisions with the wall molecules so that it loses memory of the incident velocity and emerges with a velocity characteristic of the wall temperature. We revisit this problem with molecular dynamics simulations – as the properties of the wall are varied, we find both kinds of behaviour suggested by Maxwell, but the crossover from one to the other is not as simple as envisioned by him. In addition, rich behaviour is found in the fluid flow properties on varying the fluid density from the dense liquid regime to the Knudsen regime (large mean free path compared to the system size). Our studies of flows in the subcontinuum regime provide a unique window on the nature of boundary conditions at a fluid - solid interface and are relevant to the behaviour of nanoscale mechanical devices, high altitude aerodynamics, aerosol dynamics, isotope separation schemes, flow cooling techniques, and energy transfer in molecular collisions [3–6].

Studies of flows at nanoscales involve questions pertaining to a sub-continuum regime [7,8] for which experiments are often unable to provide the requisite answers. The behaviour of materials at the nanoscale is often quite different from that in the bulk [9–12]. Numerical simulations based on molecular dynamics (MD) offer a natural tool to handle the interacting many-body nanoscale physics. A detailed understanding of the behaviour of materials at very small scales is necessary for the fabrication of miniature devices and for the manipulation of materials at the molecular scale. Such microscopic studies are useful for assessing the range of validity of traditional continuum theories. In addition, atomistic simulations are an invaluable tool for deducing constitutive relationships, which may then be fed into continuum calculations.

Here, we report on MD studies of the boundary conditions in single-fluid flows in the Knudsen regime [13] in which the mean free path, λ , becomes comparable to the characteristic device dimension, L . Such flows behave very differently from bulk, continuum expectations. There is considerable work on the modified boundary conditions based on either semi-heuristic

kinetic theory arguments or using an analysis of the Boltzmann equation, but inevitably severe simplifications are made concerning the dynamics of the system [14]. Furthermore, in such treatments, the solid boundaries are not handled in a realistic manner as having atomic structure on length scales comparable to that of the fluid constituents [15,16].

We study Lennard-Jones fluids undergoing two kinds of flow, Couette and Poiseuille, between two solid walls with an atomic structure. Three kinds of walls, two attractive and one repulsive, are discussed. We consider a range of fluid densities to study the crossover from flows described by continuum fluid mechanics to dilute gas flows in the Knudsen regime.

In a Lennard-Jones fluid, two atoms separated by a distance r interact with the potential

$$V_{LJ}(r) = 4\epsilon \left[\left(\frac{r}{\sigma} \right)^{-12} - \left(\frac{r}{\sigma} \right)^{-6} \right] , \quad (1)$$

where σ is the size of the repulsive core [the potential is truncated at 2.2σ]. The flows take place between two solid planar walls parallel to the xy plane with periodic boundary conditions imposed along the x and y directions. Couette flow was generated by moving the walls at constant velocity in opposite directions along the x -axis whereas Poiseuille flow was induced by an application of uniform acceleration g on all the fluid molecules in the x -direction.

Following Thompson and Robbins [17], the wall of atoms form two [001] planes of an fcc lattice with each wall atom tethered to a fixed lattice site by a harmonic spring of spring constant k . Our studies were done for $k=400$ so that the mean-square displacement about the lattice sites did not exceed the Lindemann criterion for melting but was close to the value set by this criterion. The wall fluid interactions were modelled by another Lennard-Jones potential,

$$V_{wf}(r) = 16\epsilon \left[\left(\frac{r}{\sigma} \right)^{-12} - A \left(\frac{r}{\sigma} \right)^{-6} \right] , \quad (2)$$

with the parameter A varying between 1 and 0, corresponding to attractive and repulsive walls respectively. For the narrowest channel that we studied, the fluid atoms were confined to a space measuring 13.6σ by 5.1σ in the xy plane and 12.75σ between the walls. The

“basic” walls in our studies contain 96 wall atoms each (in each wall plane, the atomic periodicity is 0.85σ). We have also considered the case of walls which are about 2.5 times denser and consist of 176 wall atoms each – we shall refer to these as “dense” walls.

The equations of motion were integrated using a fifth-order Gear predictor-corrector algorithm [18] with a step size of 0.005τ , where $\tau = (m\sigma^2/\epsilon)^{1/2}$ and m is the atomic (wall and fluid) mass. The fluid and wall temperatures were fixed at $k_B T/\epsilon=1.1$. We present results obtained with the use of Langevin thermostat [19] but the results obtained with the use of the Nose-Hoover thermostat [20,21] were virtually identical. The noise was applied in all directions during equilibration and only in the y -direction during the data-taking phase. The averages were obtained over runs which lasted at least 5000τ , and in the extreme dilution case, for up to 400000τ . An initial time of at least 400τ was spent for equilibration. The spatial averaging was carried out in slabs of width $\sigma/4$ along the z -axis.

In the dilute gas limit, the Knudsen number, Kn , is defined as λ/L , i.e., as $(\sqrt{2}\pi\rho\sigma^2L)^{-1}$, where λ is the mean free path, ρ is the fluid number density and L is the characteristic width of the channel. A study of the density profile shows qualitatively different behaviours of the density profiles for the attractive and repulsive walls. In the former case, two adsorbed layers form near both walls whereas there is merely a depletion zone, whose thickness is of order σ , alongside the repulsive walls. The first layer at the attractive walls is fairly periodic, as measured by the static structure factor, and the resulting local order corresponds to either a square or hexagonal lattice depending on whether the wall is basic or dense. L is defined as an effective channel width in which the flow takes place (in the attractive case this is the distance between centers of the second layers). In the center of the channel, the fluid density is essentially constant and this value is chosen as ρ in the definition of Kn .

Figure 1 shows the Poiseuille flow velocity profiles for three different values of ρ (or Kn) for the attractive wall case. We have confirmed with studies of channels of three different widths and the two wall densities that the crossover value of ρ above which continuum fluid mechanics holds, ρ_K , is somewhat less than 0.19, corresponding to a Kn of order 0.1 for the channel of the smallest width. In this regime, the profiles are clearly parabolic and essentially

with no slip at the walls. In contrast, the velocity profile at the highest Kn that we were able to study (corresponding to just 4 particles in the interior of the channel) is almost that of plug flow with a huge slip length. For repulsive walls, the plug flow regime extends to higher densities because such walls provide little coupling to the fluid and correspondingly, ρ_K becomes of order 0.3. Furthermore, in the continuum regime, the velocity field exhibits substantial slip. A consistent behaviour is found for Couette flow with higher slip for the repulsive walls (compared to the attractive wall case) for $\rho > \rho_K$ and essentially zero fluid velocity at the walls at the highest Kn .

We now proceed to study the effect of interactions between the fluid particles undergoing Poiseuille flow on increasing ρ within the channel. In Poiseuille flow, the velocity field is highest in the middle of the channel and is denoted by v_{\max} . At the lowest densities, one expects that v_{\max} ought to scale as L . This is because the driving force is effective in accelerating the fluid particles only during the time spent traversing the channel between collisions with the walls (and the associated adsorbed layers). This time simply scales as the channel width. On the other hand, at large ρ , corresponding to usual fluid behaviour, v_{\max} ought to scale as L^2 as given by the Navier-Stokes equation with no-slip boundary conditions. Figure 2 shows a plot of how v_{\max} interpolates between the low and high Knudsen number behaviours as the fluid density is varied. Strikingly, v_{\max} shows a maximum around ρ_K with the peak being more pronounced for larger L 's. We have confirmed that this qualitative behaviour is essentially independent of the nature of the walls. Physically, ρ_K corresponds to the situation when the fluid intermolecular interactions begin to dominate leading to a diminished influence of the wall in the interior of the fluid.

Figure 3 shows a vivid illustration of the role played by the intermolecular interactions in leading to an enhancement of v_{\max} even as the fluid density is moderately increased from the high Kn limit. For a repulsive wall (not shown), the particle is reflected approximately specularly and moves out of the vicinity of the wall immediately. The bottom panel shows qualitatively different behaviour in the (basic) attractive wall case. Here, again as suggested by Maxwell, a particle either thermalizes in the vicinity of the wall for a relatively long time

and then escapes from it or occasionally still undergoes specular reflection. On increasing the fluid density, one gets the situation illustrated in the middle panel in which intermolecular collisions keep the particles longer within the channel thus reducing the time of localization near the walls and effectively increasing the velocity field in the middle of the channel (Figure 2). At still higher densities ($\sim \rho_K$), the intermolecular interactions become sufficiently large so that liquid-like behaviour sets in and v_{\max} begins to decrease.

A key quantity that characterizes the fluid solid interface is the collision kernel [14,22] – the probability density that a molecule striking the surface with a given velocity reemerges with a specific velocity after a given residence time. For the repulsive wall, we find that Maxwell’s specular reflection scenario holds exceedingly well and the residence time is negligible. On the other hand, for the attractive walls the distribution of residence times develops a long tail. Strikingly, the velocity distribution of a particle after the collision with the wall is substantially independent of the incoming velocity. As an illustration, Figure 4 shows the case of particles with unit speed incident normal to the wall. The inset shows the probability distribution of residence times whereas the main figure shows the distributions of the normal (z) and tangential (x) velocities of the scattered molecules. The results are in excellent accord with Maxwell’s thermal wall scenario in which the probability densities corresponding to v_x and v_z are [1,13,23]

$$\phi_x(v_x) = \sqrt{\frac{m}{2\pi k_B T}} \exp\left(-\frac{mv_x^2}{2k_B T}\right) \quad (3)$$

and

$$\phi_z(v_z) = \frac{m}{k_B T} v_z \exp\left(-\frac{mv_z^2}{2k_B T}\right) \quad (4)$$

respectively. As expected for a thermal wall, the residence time is found to be uncorrelated with the outgoing velocity.

How does the behaviour crossover from that of specular reflection to that of a thermal wall? Following Maxwell¹, a common hypothesis is a linear combination of both behaviours with weights $(1 - f)$ and f respectively. Such an intermediate case is realized, e.g., on considering the scattering from a wall with the wall-fluid potential given by Eq. 2 with $A=1/4$.

The velocity distributions of the scattered particles clearly deviate from pure thermal behaviour and the data might be interpreted as containing a specular component. However, the resulting distributions are more complex than the simple linear combination form [24]. The behaviour of the collision kernel is further enriched on considering the role of the interactions between the fluid molecules as the Knudsen number decreases to a value of 0.27 corresponding to a density of $\rho = 0.066$ (figure 5). The influence of other fluid molecules leads to the distributions more closely approaching the thermal ones. The nature of the boundary conditions at a fluid-solid interface is thus complex but akin to those envisioned by Maxwell.

We are indebted to Mark Robbins and Riina Tehver for many valuable discussions. This work was supported by KBN (Grant No. 2P03B-025-13), NASA, and the Petroleum Research Fund administered by the American Chemical Society.

REFERENCES

- [1] J. C. Maxwell, *Phil. Trans. R. Soc. London. Ser. A* **170**, 231 (1867)
- [2] J. C. Maxwell, *Phil. Mag.* **19**, 20 (1860)
- [3] E. P. Muntz, D. Weaver, and D. Campbell, eds., *Rarified Gas Dynamics*, (American Institute of Aeronautics and Astronautics, Washington, 1989)
- [4] C.-J. Kim, ed., *Microelectromechanical systems (MEMS)*, (American Society of Mechanical Engineers, New York, 1997)
- [5] W. H. Marlow, ed., *Aerosols: Aerosol Microphysics I - Particle Interactions*, (Springer, New York, 1980)
- [6] W. Ehrfeld, *Elements of Flow and Diffusion Processes in Separation Nozzles*, (Springer, New York, 1983)
- [7] J. Koplik and J. R. Banavar, *Computers in Physics* **12**, 424 (1998)
- [8] J. Koplik and J. R. Banavar, *Annu. Rev. Fluid Mech.* **27**, 257-92 (1995)
- [9] S. Sugano, *Microcluster Physics*, (Springer, Berlin, 1991)
- [10] B. Bhushan, J. N. Israelachvili, and U. Landman, *Nature* **374**, 607 (1995)
- [11] I. Bitsanis, T. K. Vanderlick, M. Tirrel, and H. T. Davis, *J. Chem. Phys.* **89**, 3252 (1988)
- [12] W. Loose and S. Hess, *Rheol. Acta* **28**, 91 (1989)
- [13] E. H. Kennard, *Kinetic Theory of Gases*, (McGraw-Hill, New York, 1938)
- [14] C. Cercignani, *The Boltzmann Equation and its Applications* (Springer, Berlin, 1988)
- [15] D. K. Bhattacharya and G. C. Lie, *Phys. Rev. A* **43**, 761 (1991)
- [16] D. L. Morris, L. Hannon, and A. L. Garcia, *Phys. Rev. A* **46**, 5279 (1992)

- [17] P. A. Thompson and M. O. Robbins, *Phys. Rev. A* **41**, 6830 (1990)
- [18] See, e.g. M. P. Allen and D. J. Tildesley, *Computer Simulation of Liquids* (Clarendon, Oxford, 1987)
- [19] G. S. Grest and K. Kremer, *Phys. Rev. A* **33**, 3628 (1986)
- [20] S. Nose, *Mol. Phys.* **52**, 255 (1984)
- [21] W. G. Hoover, *Phys. Rev. A* **31**, 1695 (1985)
- [22] Y. Matsumoto, N. Yamanishi and H. Shobatake, *Proceedings of the 19th International Symposium on Rarefied Gas Dynamics*, 995 (1994)
- [23] R. Tehver, F. Toigo, J. Koplik, and J. R. Banavar, *Phys. Rev. E* **57**, R17 (1998)
- [24] The velocity distributions in this case are shown (figure 10) in a conference paper, M. Cieplak, J. Koplik, and J. R. Banavar, *Physica A* **274**, 281 (1999). The complementary case of a repulsive wall is considered in detail in this work and the results are benchmarked against our basic findings presented here.

Figure captions

FIG. 1. Velocity profiles of Poiseuille flow with $g = 0.01\sigma/\tau^2$ for the smallest width channel with basic attractive walls. The values of the interior fluid density and the corresponding Knudsen number are indicated. The filled circles denote the highest Kn case. The inner wall layers are at the edges of the figure. Effectively, one observes no slip boundary conditions for the two higher density cases (the slip length is around 1.7σ measured with respect to the wall location, but note the presence of the adsorbed layers at the wall).

FIG. 2. Plot of the fluid velocity in the middle of the channel in Poiseuille flow with $g = 0.01\tau/\sigma^2$ as a function of fluid density (and the Knudsen number in the inset). The plot is for three different channel widths. The L_0 in the figure denotes the narrowest channel. For this case, both attractive walls were considered – the basic (hexagons) and higher (asterisks) wall densities. $2L_0$ and $4L_0$ denote channels that are effectively twice and four times as wide as the smallest channel.

FIG. 3. Plot of the time dependence of the z -coordinate of a typical fluid particle undergoing Poiseuille flow in the narrowest channel. The horizontal dotted lines indicate the z -coordinates of the wall molecules. The solid horizontal line refers to the centers of the adsorbed first layers.

FIG. 4. The probability density distributions for the z (normal) and x components of the outgoing velocity of a fluid molecule after collision with the wall and the associated adsorbed layer. The solid histograms are obtained based on 3000 scattering events. The dotted lines are the analytic predictions of Maxwell, eqs. 3 and 4, discretized with a bin size of $0.1 \sigma/\tau_0$ as in the simulations. The inset shows the distribution of residence times. The residence time is measured as the time interval between a fluid molecule leaving a force-free

region (near the wall) and its reemergence. The peak of the curve (at a non-zero value of τ) corresponds to a virtually instantaneous bounce back of the fluid molecule and accounts for the time needed to approach the wall and return.

FIGURES

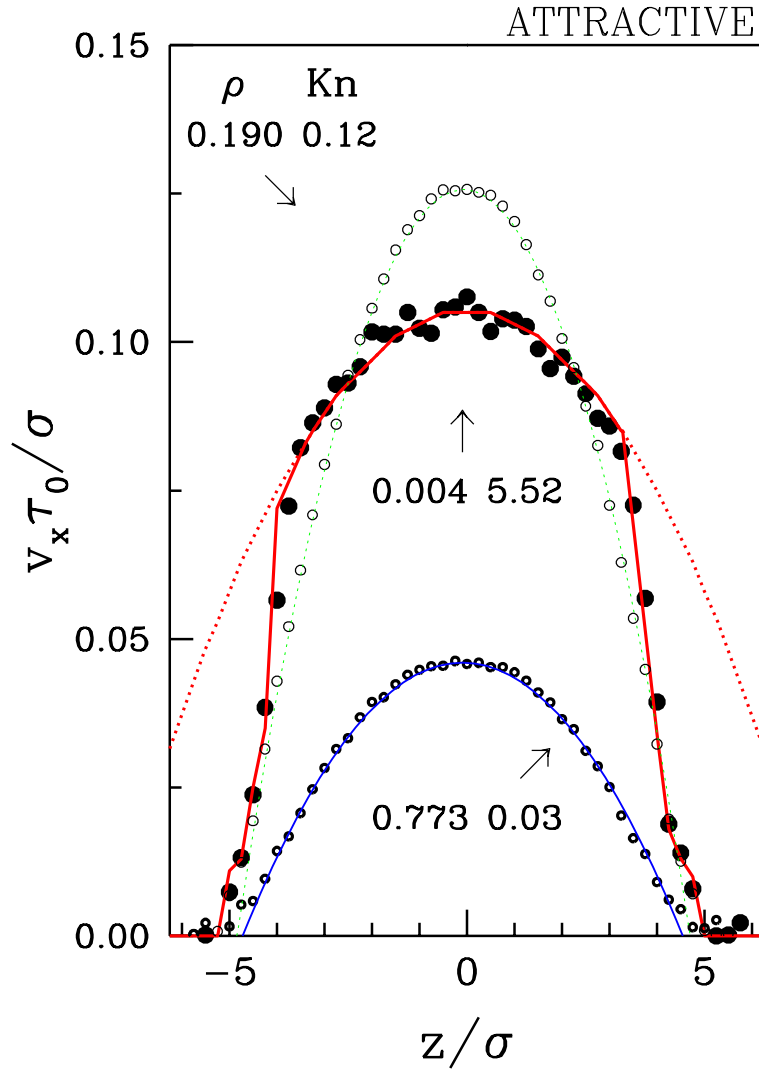


FIG. 1.

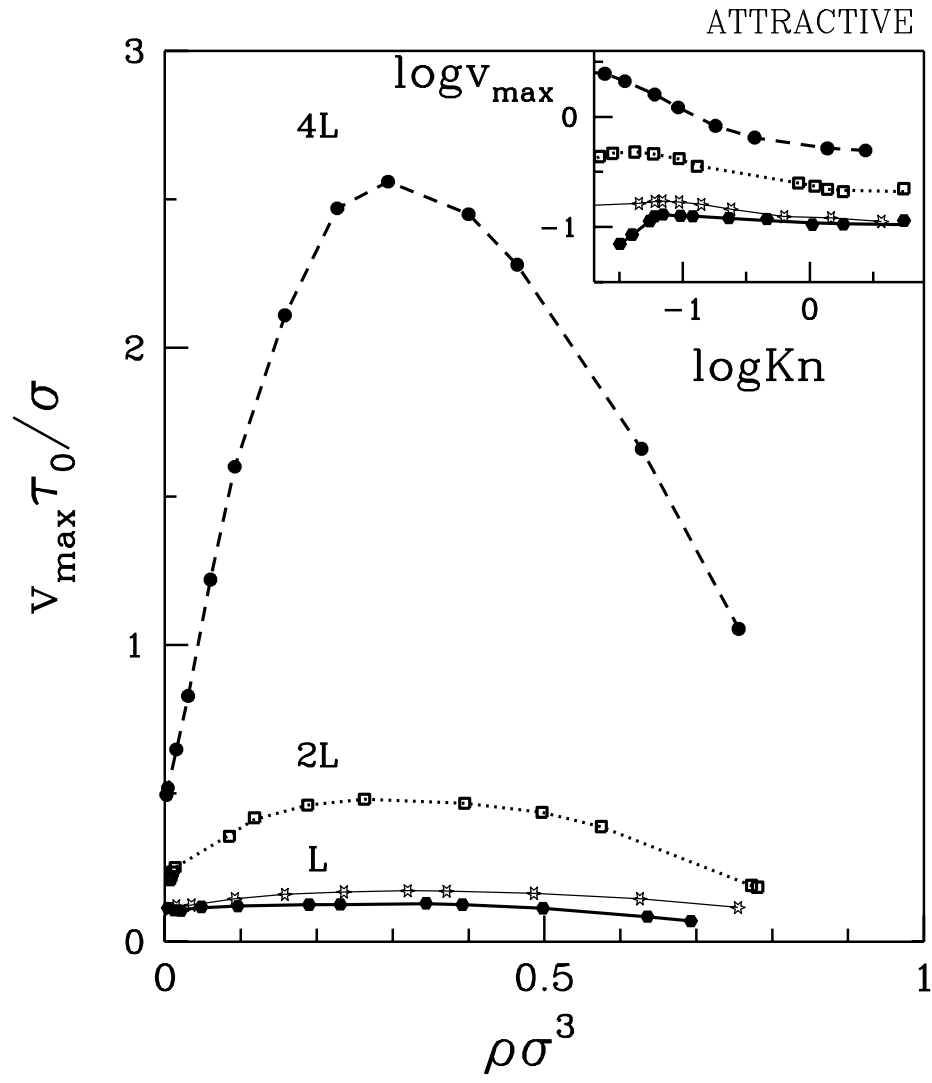


FIG. 2.

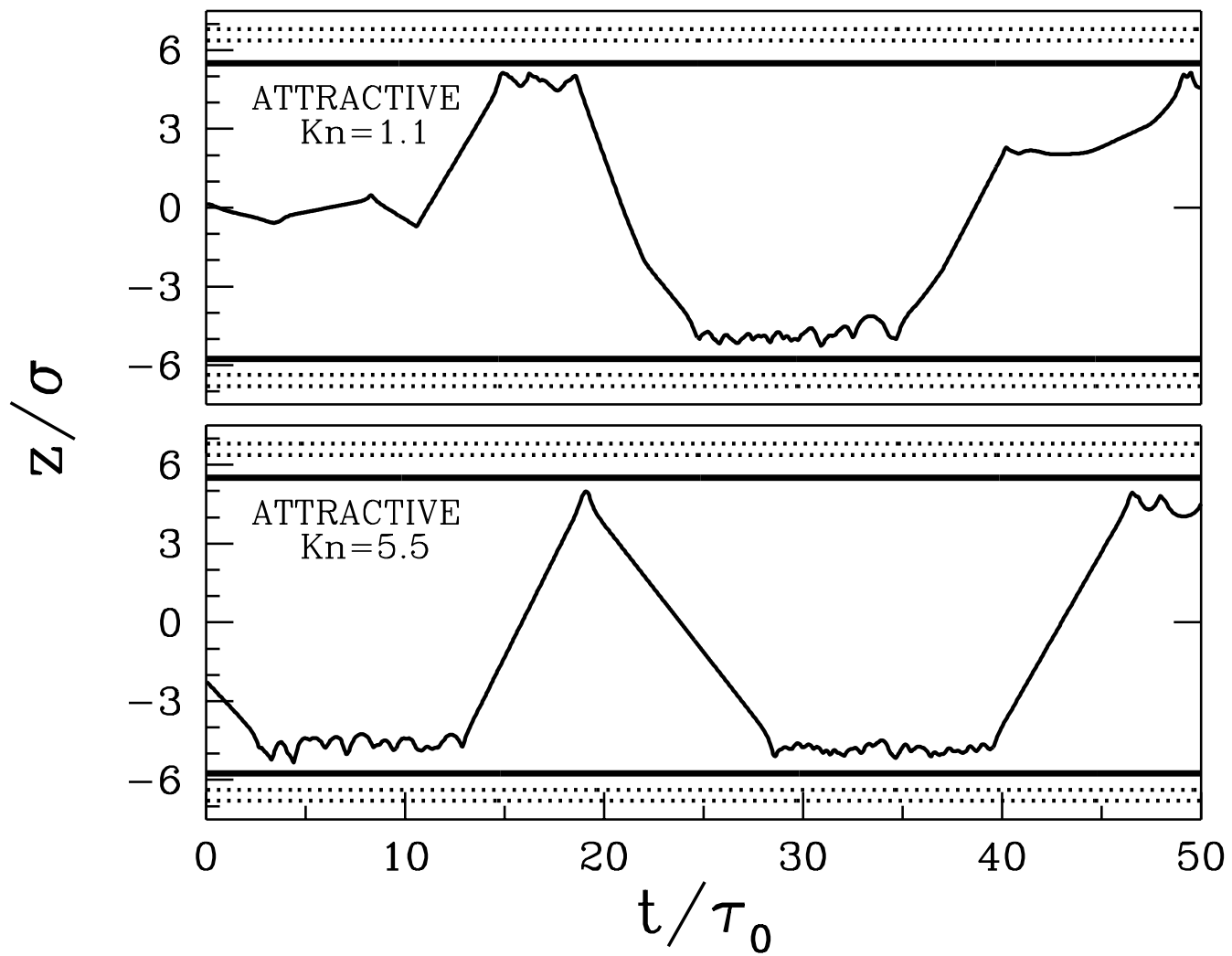


FIG. 3.

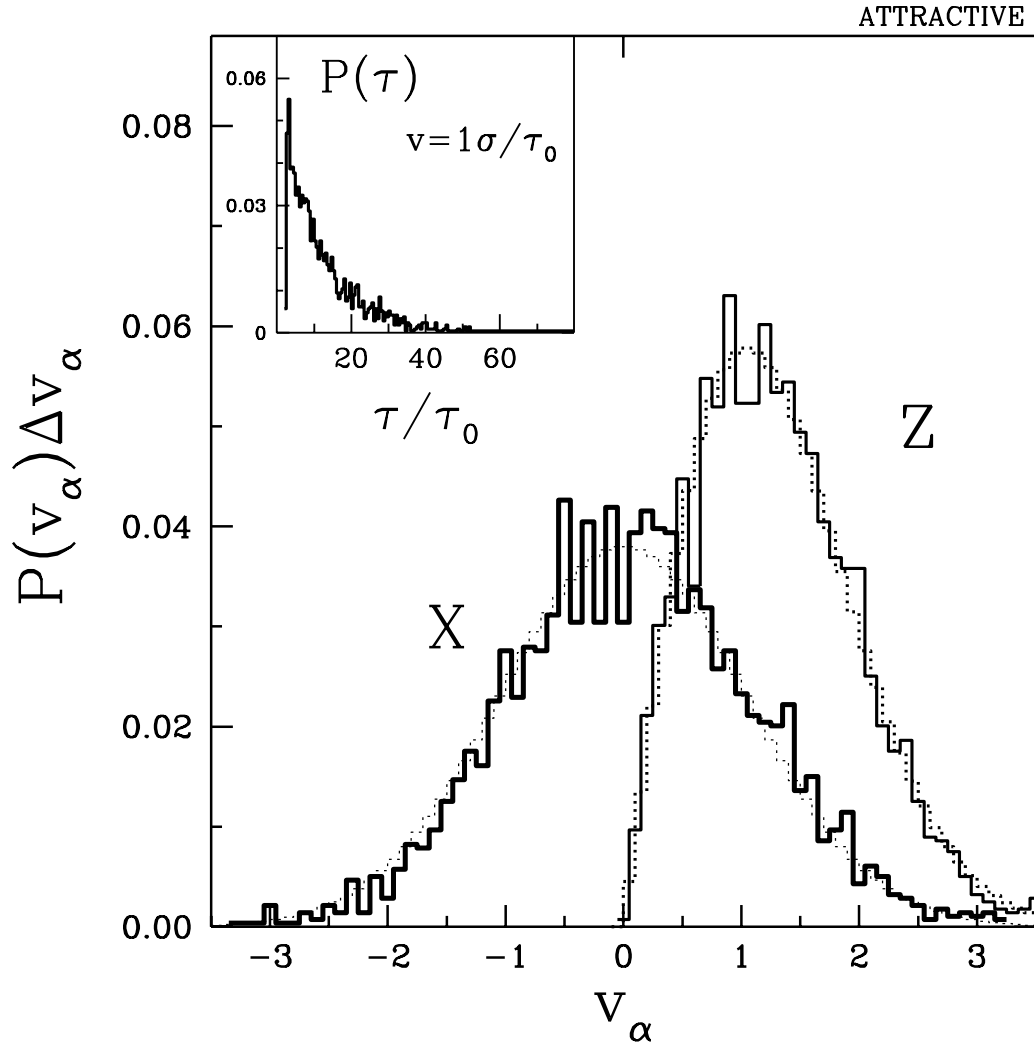


FIG. 4.